A Machine-Learning-Assisted Stochastic Cloud Population Model as a Parameterization of Cumulus Convection

Samson Hagos[1] , **Jingyi Chen[1]** , **Katelyn Barber[1]** , **Koichi Sakaguchi[1]** , **Robert S. Plant[2]** , **Zhe Feng[1]** , **and Heng Xiao[1]**

[1]Pacific Northwest National Laboratory, Richland, WA, USA, [2]University of Reading, Reading, UK

Abstract A machine-learning-assisted stochastic cloud population model is coupled with the Advanced Research Weather Research and Forecasting (WRF) model to represent fluctuations in the cloud-base mass flux associated with the life cycles and interactions among cumulus convection cells. In this cloud population model, the size distribution and the associated cloud-base mass flux of the convective cells are related to their previous state and to the change in the total convective area via a transition function. The convective area tendency in turn is assumed to depend on the cloud-base mass flux that is resolved by the host WRF model. The transition function is represented by a single hidden-layer neural network trained by the evolution of convective cell size distributions in a 1-km grid-spacing WRF simulation run over the Australian Monsoon region. At every grid point of the host model, the cloud population model predicts the cell size and cloud-base mass flux distributions from which a random sample of cells is fed to an entraining parcel model that calculates precipitation as well as the associated liquid water potential temperature and total moisture tendencies. These tendencies are averaged over the cells and provided to the host model. Several regional simulations are performed over tropical and midlatitude domains to test this as a potential approach to scale-aware parameterization. It is shown that such an approach could be a new promising path to simulating realistic precipitation statistics and propagation of precipitation associated with the Madden-Julian Oscillation while maintaining realistic depictions of the diurnal cycle over both land and ocean.

Plain Language Summary A stochastic cloud population model is coupled with a Weather Research and Forecasting model for applications as a parameterization of cumulus convection. The model predicts the evolution of the cloud-base mass flux distribution via a transition function obtained using the machine learning algorithm trained by a 1-km grid-spacing convection permitting model simulation. The predicted mass flux statistics is then provided to an entraining plume model to obtain heating and moistening tendencies. The potential of the approach as a path to improvement of statistics and variability of precipitation in models is examined over multiple regimes.

1. Introduction

The expansion of computational resources and numerical methodologies has allowed global weather forecasting and experimental climate models to run with horizontal grid-spacings of 10s of kilometers or less. But this opportunity comes with the requirement to re-examine the treatment of subgrid convection processes. Traditionally climate models, which typically run at a grid spacing of 100 km or more, relied on cumulus parameterizations, which implicitly or explicitly assume a "quasi-equilibrium" (QE) balance between large-scale (resolved) forcing and convection. Under the QE assumption, low-level heating and moistening along with upper-level radiative cooling and other processes that destabilize the troposphere are assumed to be in balance with the net large-scale effects of unresolved, convective cloud processes, including upper-level warming and boundary-layer drying (Arakawa & Schubert, 1974; Emanuel, 1994). These assumptions, while reasonable for coarse grid-spacing and under slowly varying conditions, fail for high-frequency variability from forcings such as the diurnal cycle and for the organized convection that covers areas comparable to the grid cell size such as MCSs (Jones & Randall, 2011; Xu et al., 1992). At grid spacings of order 1 km, convection-permitting simulations have proved valuable, typically for local or regional scales (Clark et al., 2016; Poujol et al., 2020). However, neither traditional parameterization nor explicit modeling is optimal for the intermediate grid-spacing models (Arakawa & Wu, 2013; Gerard, 2015).

Several approaches have been proposed to address the issue of representation of variability associated with life-cycles of the convection and interactions among clouds. Reviews are provided by Rio et al. (2019), Goswami
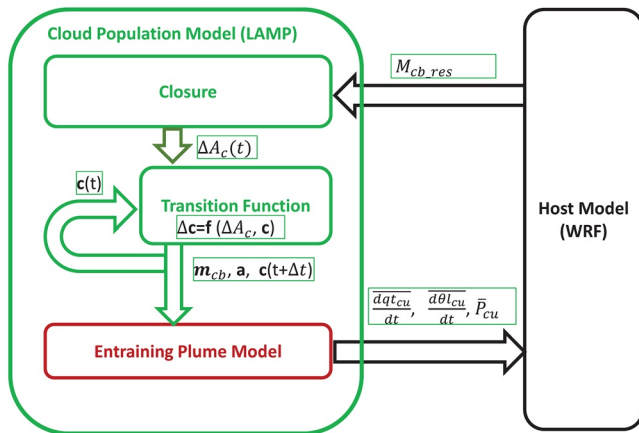
Figure 1. The schematic of the coupling of the Learning-Assisted Model for Parameterization scheme with Weather Research and Forecasting. All symbols are explained in the main text.

et al. (2017), S. Hagos et al. (2018), and S. Hagos et al. (2020), and only a summary of relevant points is given here. One approach is to introduce stochasticity into parameterizations with a prescribed distribution of the mass flux or the convective area (Khouider et al., 2003; Plant & Craig, 2008; Teixeira & Reynolds, 2008; Wang et al., 2016, 2021). Alternatively, noise has been introduced to the heating/moistening tendencies or to state variables in GCM vertical columns (Davini et al., 2017) in some schemes. Yet another approach put forward by Majda and Khouider (2002) and Khouider et al. (2010) is a stochastic multicloud representation based on the Markov process on a subgrid lattice.

In our recent paper, S. Hagos et al. (2018), a stochastic prognostic model for the population dynamics of convective clouds was proposed. The model takes a nonequilibrium statistical mechanical approach to represent the evolution of the size distribution of convective cells and their associated cloud-base mass flux. At the core of the model is a transition function that relates the size distribution of convective cells at a given time to a previous state and to a given change in the total convective area in the box. The transition function was derived from physical and probabilistic arguments. In a follow-up study, S. Hagos et al. (2020), it was shown that such a transition function can also be directly derived from C-band radar observations of precipitating clouds via machine learning. In that study, the use of the transition function was extended to construct a simple model for describing the interactions between convective and stratiform clouds. The present study explores the potential applications of the ideas developed by S. Hagos et al. (2018, 2020) for the development of stochastic cloud population model-based cumulus parameterizations that can represent precipitation statistics in a regional mesoscale model at grid spacings between 25 and 1 km. The next section presents a description of the cloud population model (Sections 2.1–2.3) and its coupling to the mesoscale model (Section 2.4). Section 3 examines the impacts on precipitation statistics, the spatial distribution and diurnal cycle of precipitation, and precipitation propagation as part of Madden-Julian Oscillation events. The implications of the study are discussed in Section 4.

2. Development

2.1. Design

The overarching design of the cloud population model and its coupling to the host model is depicted in the schematic in Figure 1. The forcing to the cloud population model is provided by the resolved cloud-base mass flux (M_{cb_res}) in a grid box of the host model. Specifically, we will use the Weather Research and Forecasting (WRF; Skamarock et al., 2008) version 4.0 model for the tests below but the method could straightforwardly be applied to other host models with appropriate modification to the closure depending on the grid spacing of interest. The cloud population model applies a closure assumption to calculate in turn the change in the total convective area ΔA_c in the grid box. The closure is presented in Section 2.4.

The cloud population is divided into N bins of the cloud-base mass flux, with a subscript i being used henceforth to denote a bin label. In the practical implementation for this study, we choose $N = 30$ bins, with the mean cloud-base mass flux in each bin exponentially increasing from a minimum of $m_{cb(1)} = 0.2 \text{ kgm}^{-2}\text{s}^{-1}$ to $m_{cb(30)} = 1.4 \text{ kgm}^{-2}\text{s}^{-1}$. These values correspond to the minimum m_{cb} used to define a mass flux object in the WRF-CPM training simulation (Section 2.3) and to the maximum value obtained from the simulation. Precipitation from objects within this range accounts for almost all of the precipitation in the WRF-CPM domain.

c is a vector whose i^{th} element is the total convective area associated with convective cells in the bin with a mean cloud-base mass flux of $m_{cb(i)}$. Therefore, the total convective area in a grid box is given by $A_c = \sum_{i=1}^{N} c_i$. The mean cell area for the ith bin, denoted as a_i, is constant and obtained by taking the average of the sizes of all cells in the mass flux bin $m_{cb(i)}$. Thus, $c_i = n_i a_i$ where n_i is the number of distinct cells in the bin.

For the given change in the total convective area (ΔA_c), the change in c is assumed to be given by

$$\Delta c = f(c)\Delta A_c \tag{1}$$

where $f(c)$ is the transition function that allocates the change in the convective area to the different mass flux bins. It is obtained from a 1-km grid-spacing simulation using machine learning as discussed in Section 2.2. Once c is advanced forward, and the new mass flux distribution is obtained, the frequency of the convection is regulated by a stochastic variable ε with a value of one or zero with a given probability p. If ε is 1, for a given nonzero c_i, a_i and $m_{cb(i)}$ are passed on to the cloud model, that is, the convection is activated. This results in a subsample $m \leq N$ cells being passed to the cloud model. This is motivated by the fact that the domain of the cloud population model is much larger than the actual model grid box. Thus, stochasticity is introduced as a natural representation of the movement of clouds into and out of the grid box of interest. Before continuing with the development, a brief discussion of the relationship of this model, specifically Equation 1 with the STOMP model discussed in S. Hagos et al. (2018) is warranted. The model presented here is a generalization of STOMP in that it includes nonlinear interactions among clouds of varying sizes. In STOMP, the diagonal of a transition matrix T_{ij} was populated using simple physical arguments to relate the probabilities of growth of a cell to its current size. In the current version of the cloud population model however, the transition function $f(c)$ is a more complex nonlinear function such that the probability of growth of a cell depends not only on its previous size but also on the size distribution of all cells in the domain.

When the convection is activated within a bin, $m_{cb(i)}$ and a_i are provided as inputs to an entraining plume model, which calculates the convective total water tendency $\left(\frac{dqt_{cu}}{dt}\right)_i$ and liquid water potential temperature tendency $\left(\frac{d\theta l_{cu}}{dt}\right)_i$ as well as precipitation P_{cui} from each m_{cb} bin. The final convective tendencies on the mesoscale model grid are then calculated as

$$\overline{\frac{d\theta l_{cu}}{dt}} = \sum_{i=1}^{m} \frac{c_i}{A_{gb}} \left(\frac{d\theta l_{cu}}{dt}\right)_i, \tag{2}$$

$$\overline{\frac{dqt_{cu}}{dt}} = \sum_{i=1}^{m} \frac{c_i}{A_{gb}} \left(\frac{dqt_{cu}}{dt}\right)_i, \tag{3}$$

and

$$P_{cu} = \sum_{i=1}^{m} \frac{c_i}{A_{gb}} Pcu_i \tag{4}$$

where A_{gb} is the area of the grid box.

In the next three subsections, the simulations performed as part of the development (Section 2.2), the machine learning algorithm (Section 2.3), and the closure (Section 2.4) are discussed. As it is not central to the work, the detailed description of the entraining plume model used to calculate the moisture, heating tendencies, and precipitation is provided in the Appendix A. Hereafter, the cloud population model being used as a cumulus parameterization will be referred to as the machine Learning-Assisted Model for Parameterization of convective cloud populations (LAMP).

2.2. Development Simulations

In the development of the scheme, five supporting WRF simulations are performed, and these are described here. For all the simulations, lateral boundary and surface conditions, including sea-surface temperature, are obtained from ERA5 (Copernicus Climate Change Service [C3S], 2017) and are updated every 6 hr. The first simulation has 1-km grid spacing and covers the month of January 2006, an active phase of the Australian monsoon season. The purpose of this simulation is to obtain the training data for the cloud-base mass flux. This simulation is hereafter referred to as WRF-CPM (1 km). Before describing the other simulations, the choice of 1-km grid-spacing simulation for training must be justified. It has been shown that to fully resolve mass flux fluctuations in the convection, grid spacings of 250 m or less are required (e.g., Bryan et al., 2003; Heinze et al., 2017). Since the objective of this work is to demonstrate the potential of this approach and its key feature is the representation of the evolution of a large population of convective clouds over water and land, the large domain and hence
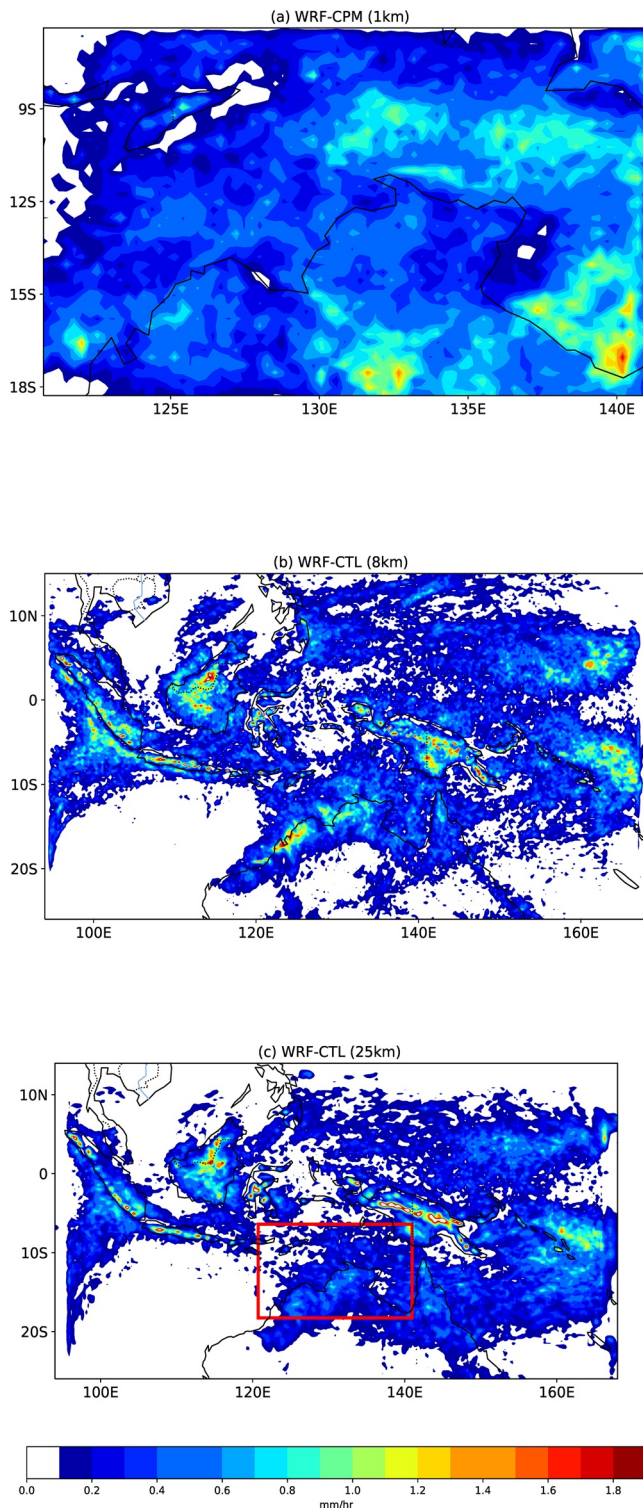
Figure 2. The domains of the three simulations used in development along with the mean precipitation from a month long control (WRF-CTL) simulations; (a) the small domain 1.0-km grid-spacing simulation used for training, (b and c) large domain 8 and 25-km grid-spacing simulations. The red box in panel (c) indicates the domain of the training simulation relative to the large domain.

relatively coarse grid-spacing is necessary due to computational resources constraints. In our previous work (S. Hagos et al., 2014), the performance of such kilometer-scale simulations in representing radar observed precipitating cloud population statistics is extensively documented. It was shown that the WRF model represents well the statistics of the convective area distribution, the relationship between echo-top height and cell area, and cold pool properties. Ideally, one would perform multiple training simulations to cover regions with diverse environmental conditions. In fact, one can even imagine using global convection permitting (km scale) simulations like those under development in the DYAMOND project (Stevens et al., 2019) for training applications. As computational resources increase, one could also envision performing a development like that proposed here based on such sub-km grid-spacing simulations over multiple regions. As will be discussed in the evaluation section, the use of convection permitting simulations as ground truth comes with its own challenges. One has to acknowledge the biases associated with the treatment of a microphysical and boundary layer and other processes in such simulations.

The second and third simulations are similar but with larger domains and run at 8-km and 25-km grid spacings. They are referred to as WRF-CTL (8 km) and WRF-CTL (25 km), respectively. In all these three simulations, cumulus parameterization is turned off and the time steps for the three simulations are 4, 30, and 100 s, respectively. The domains for these simulations are shown in Figure 2. The 8 and 25-km grid-spacing simulations are also repeated with LAMP coupled with WRF and these are referred to as WRF-LAMP (8 km) and WRF-LAMP (25 km), respectively. All the simulations are centered at Darwin, Australia (12.46°S and 130.85°E) and include both tropical ocean and land conditions. The last four simulations at coarser resolutions (WRF-CTL [8 km], WRF-CTL [25 km], WRF-LAMP [8 km], and WRF-LAMP [25 km]) are run for two months from 1 January to 28 February 2006. The model configuration choices that are common to all the simulations are listed on Table 1.

2.3. Determination of the Transition Function Using Machine Learning

As a first step in determining **f(c)**, the cloud-base mass flux was calculated at every grid point of the WRF-CPM (1 km) simulation at the 10-min frequency. The cloud-base height was defined as the lowest level z_{cb} for which the cloud liquid water content $q_l(z)$ is both larger than a threshold value of 10^{-5} kg kg^{-1} and was below the level of peak $q_l(z)$. Then, the cloud-base mass flux at each grid point was calculated as

$$m_{cb} = \rho\left(z_{cb}\right) w\left(z_{cb}\right)$$ (5)

where ρ is the density of air in kg m^{-3} and w the vertical velocity in m s^{-1}.

A convective cell is defined as a contiguous area of the cloud-base mass flux of greater than 0.2 kgm^{-2}s^{-1}. The domain is gridded into 100 by 100 km boxes as shown in the example frame in Figure 3a. Although the target grid-spacing for the LAMP parameterization is less or equal to 25 km, this larger box is selected to include a sufficient sampling of larger cells. The convective cells within the 100 km x 100 km boxes are placed into $N = 30$ bins according the mean cloud-base mass flux of their respective contiguous areas, as described in the last subsection. The bin average mass fluxes constitute the n-dimensional $\boldsymbol{m_{cb}}$ vector discussed above while the bin-average and bin-total cell

Table 1
Model Configuration (Common to All Simulations)

Longwave radiation scheme	The rapid radiative transfer model (Mlawer et al., 1997)
Shortwave radiation scheme	The rapid radiative transfer model (Morcrette et al., 2008)
Microphysics scheme	Thompson (Thompson et al., 2008)
Land surface model	Unified Noah model (Ek et al., 2003)
Boundary layer scheme	Mellor-Yamada Janjic scheme (Janjic, 2001)
Surface, initial and boundary condition data	ERA5 (C3S, 2017) updated every 6 hr
Number of vertical levels	35
Model top	50 hPa

areas are represented by the vectors a and c, respectively. Figure 3b shows the mean values of $m_{cb(i)}$ and a_i for the 30 bins. For a given 100×100 km box (Figure 3a), $c(t)$, the corresponding $\Delta c(t) = c(t + 1) - c(t)$ and ΔA_c are calculated from the 1-km grid-spacing CPM simulation for training the machine learning algorithm and determining $f(c)$ from Equation 1. The 10-min frequency of training data, motivated by the frequency of precipitation radar scans (S. Hagos et al., 2018, 2020), is found to be computationally reasonable to capture the convective variations of interest on the scale of the box. However, in the implementation of WRF-LAMP, c is evolved at the frequency of the model time-step, along with A_c.

In many ways, the machine learning algorithm developed here, shown in Figures 3c, is like that presented in S. Hagos et al. (2020). The key differences here are that (a) the bins are defined by mass flux values from the 1-km grid-spacing simulation instead of convective cell sizes from radar observations and (b) in the current implementation, the explicit prediction of the stratiform area is excluded for simplicity. A single-nonlinear-hidden layer machine learning algorithm is constructed. The hidden layer constitutes a rectified linear unit activation function that introduces the nonlinearity. A graphical depiction of the algorithm is provided in Figure 3c. The transition function is assumed to be completely defined by the pairs of weight arrays (w_0 and w_1) and bias vectors (b_0 and b_1) and given the constraint that the error (Error), defined as the sum of the squares of the difference between elements of predicted and true Δc arrays, is minimized. The code is written in TensorFlow and the Adaptive Moment Estimation optimizer (Kingma & Ba, 2015) is used in the minimization. As is standard in machine learning applications, one set of snapshots (40,000 pairs) is used for training while another set of the same size is used for testing. The results are rather insensitive to the choice of the training and validation sets.

The weights and biases that define the transition function are optimized such that the error in the predicted changes in the convective area in the given mass flux bin is minimum as discussed above. Thus, in a statistical sense, given the evolution of the total convective area, the transition function should correctly predict the evolving frequency distributions of the mass flux. Figure 4 shows the frequency distribution of the mass flux as a function of the total convective area obtained from the CPM simulation and the corresponding distribution obtained from applying the transition function to the total convective area time series. The machine learning algorithm provides a reasonable description of the mass flux distribution. At smaller values of the total convective area, the distribution is relatively broad with both weak and strong convective cells co-existing with a comparable frequency. As the total convective area becomes larger the mass flux distribution becomes narrower and has a peak at about $0.8 \ \mathrm{kg m^{-2} s^{-1}}$. There are relatively few weak cells and the convection is dominated by strong cells, as one would expect from the increased organization.

2.4. Precipitation Data Set for the Evaluation

To evaluate the model simulated precipitation over various regions and seasons in a consistent manner, the Integrated Multi-satellite Retrievals from Global Precipitation Measurement V06B (IMERG, Huffman et al., 2019) is obtained and processed. This data set has a horizontal grid-spacing of 0.1° and the frequency of half-hour with global coverage. Recent evaluations of the IMERG data set against ground-based observations have documented significant improvements over its predecessor, the Tropical Rainfall Measuring Mission (TRMM) as well as other satellite products especially over tropical land such as India (Murali Krishna et al., 2017), Africa

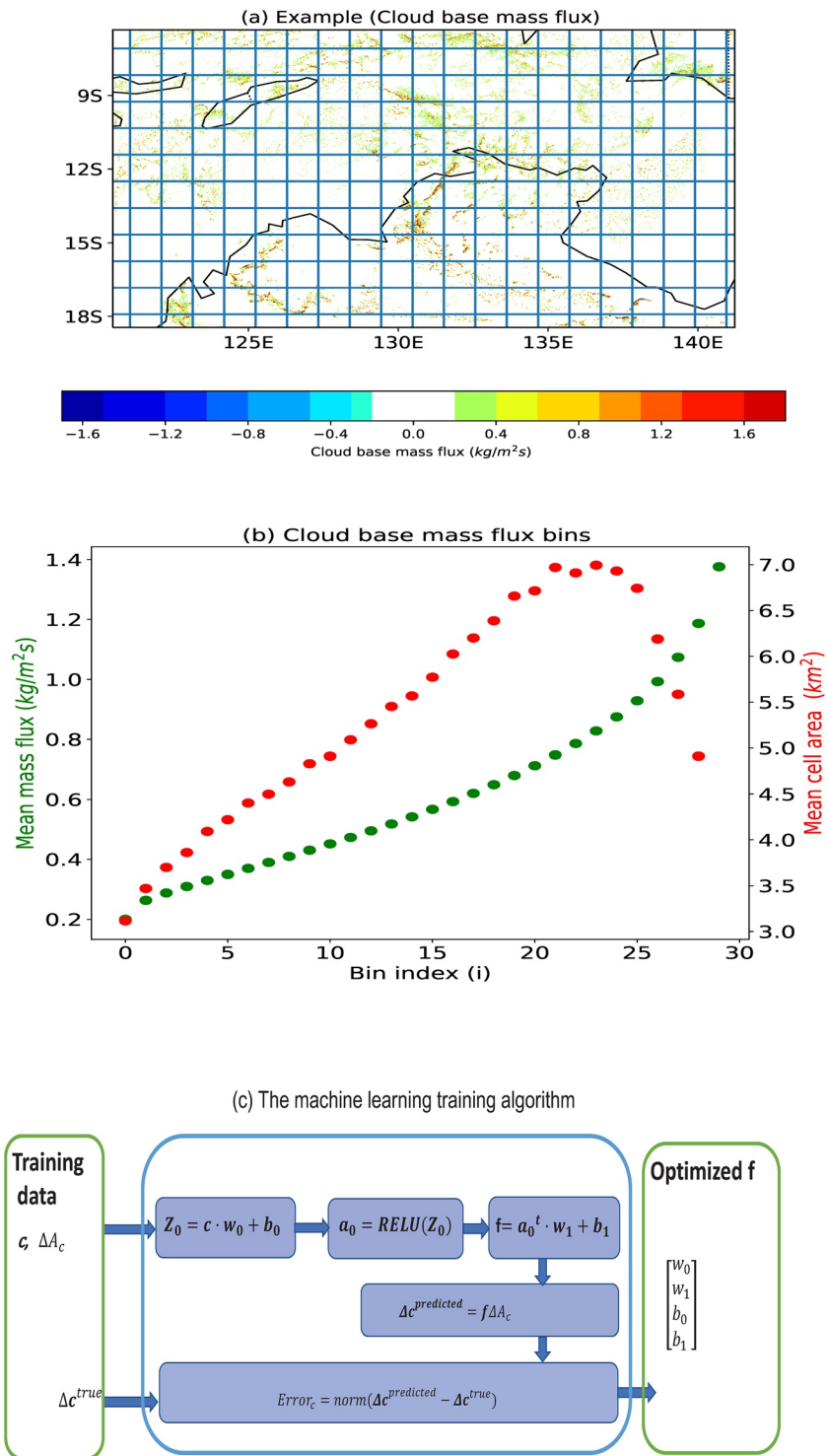**Figure 3.** (a) An example frame of cloud-base mass fluxes along with 100×100 km grid boxes from which the distribution of convective areas in mass flux bins (c_i) are obtained, and (b) the mean values of cloud-base mass fluxes (m_{cbi}) and mean cell sizes (a_i) for each of the 30 bins (see text). (c) The machine learning algorithm used to obtain the transition function from the 1-km WRF-CPM simulation.
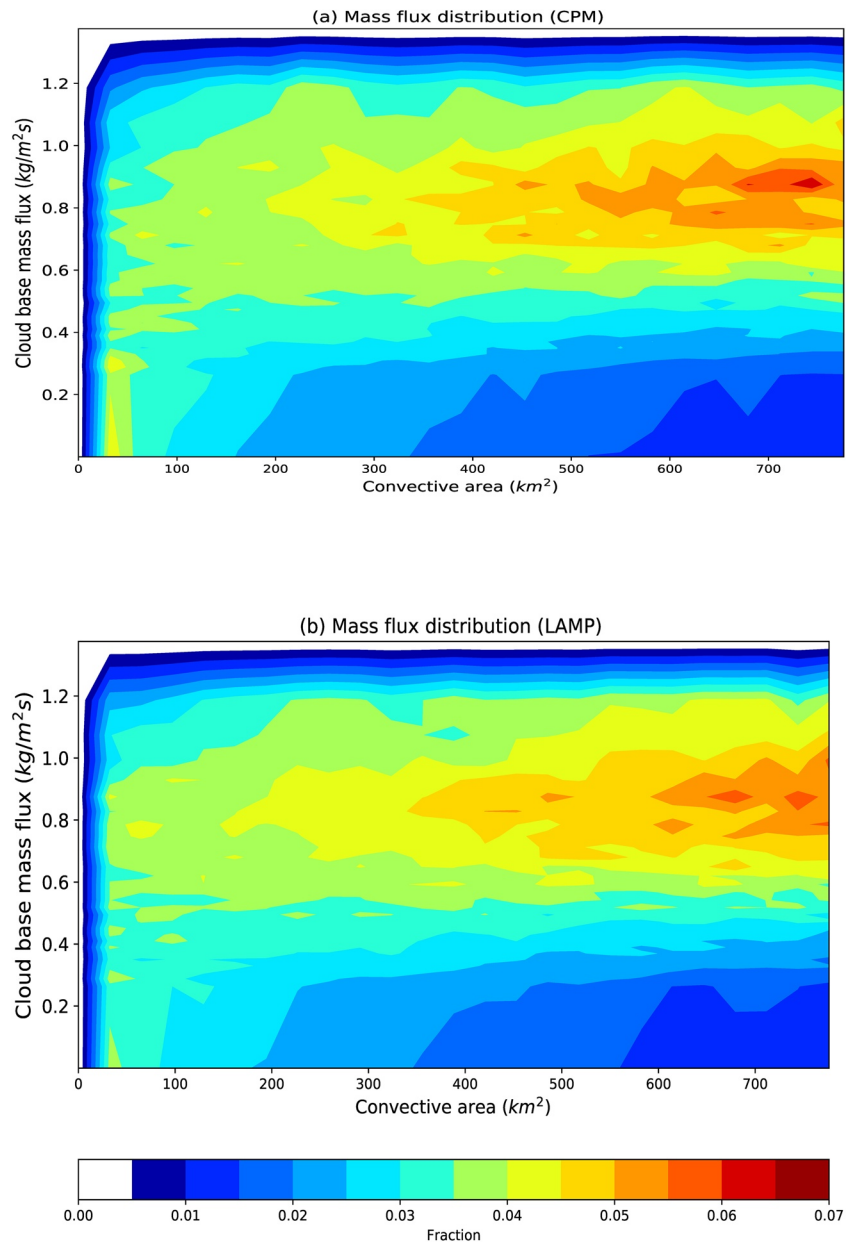
Figure 4. The frequency distributions of cloud-base mass fluxes for a given total convective area (*x*-axis) from (a) the CPM simulation compared with that obtained from (b) the machine learned transition function in Learning-Assisted Model for Parameterization.

(Dezfuli et al., 2017), Australia (Islam et al., 2020) and Taiwan (Hong et al., 2006). However, over Western Africa, it has been shown to overestimate the rainfall amount from frequently occurring weak convective events while underestimating that from rare but strong MCSs (Maranan et al., 2020). Over the continental US, on the other hand, IMERG was found to have a wet bias in total precipitation, an overestimation of the frequency of weak precipitation (<2 mm hr^{-1}), and underestimation of the frequency of intense precipitation (>10 mm hr^{-1}) in warm-season MCSs (Cui et al., 2020). The IMERG data set has been used to develop a global MCS tracking data set in a recent study (Feng et al., 2021), where it is found that maximum MCS rainfall intensity over the ocean is higher than that over land. The authors of that study cautioned that IMERG precipitation retrievals may be biased in intense convection, like those based on spaceborne radar/microwave platforms such as TRMM or GPM (Gingrey et al., 2018). While the IMERG data set is by no means perfect, it has been examined over a broad

range of environmental conditions. In this study, we use it as a benchmark for the development and evaluation of cloud-population-model-based parameterization. For the applications throughout this paper, the data set is regridded onto a 25-km grid and averaged to hourly, as are all of the precipitation data from the various simulations that it is compared to.

2.5. Coupling, Closure, and Optimization

Once the transition function is determined, the next step is coupling LAMP to the host model as shown in Figure 1. However, to do so the forcing, which is responsible for the variations in the convective area, ΔA_c must be specified according to some physically justified closure assumption. The closure we propose is motivated by the continuum nature of the statistics of precipitating convective cells over the range of scales of interest (S. Hagos et al., 2014). This implies one can assume that the presence of the resolved convection makes the presence of the unresolved convection more likely than otherwise. In other words, as the choice of the grid spacing is arbitrary, we have no physical reason to believe the large-scale environment favorable for convective cells of a given size that is marginally resolved by the grid spacing is not also favorable for cells that happened to be not large enough to be resolved. Therefore, the unresolved convective area at a given time step and location is taken to be proportional to the resolved cloud-base mass flux M_{cb_res},

$$A_c = \alpha(\Delta x) M_{cb\_res} \qquad (6)$$

where Δx is the model grid-spacing and α is a grid spacing-dependent parameter to be optimized as will be discussed below. As discussed above, the expression rests on the idea that the resolved mass flux in the mesoscale model carries valuable information about the timing, location, and rate of the development of a convective activity but that the convection needs to be partitioned between the resolved and subgrid scales. Hence, the proportionality factor can vary with the grid spacing (Δx). Thus, the parameterized convection varies similarly to that which is resolved, apart from the variability related to lifecycles of the convection and interactions among convective cells, which are represented through the transition function. In principle, the closure presented here, relating the convective area fraction to the resolved mass flux is not particularly new. Kuo (1974) proposed the linking parameterized convection to resolved moisture convergence, which by continuity can be related to the resolved mass flux. In this case, moisture is indirectly included in the definition of the cloud-base height. To assess the validity of this assumption, the relationship between convective area fraction and average cloud-base mass flux over 25 and 8-km grid boxes obtained from the WRF-CPM simulation is examined (Figure 5a). The linear relationship is quite apparent albeit with a large variance, which provides a rationale for introducing the stochastic component.

Since the objective is for the model to seamlessly represent the convection between 25-km grid spacing and 1-km grid spacing, we choose the partitioning by requiring that (a) the sum of the resolved and parameterized cloud-base mass fluxes should be insensitive to grid spacing (Δx) and (b) that the cumulus parameterization should smoothly turn itself off at the 1-km training grid-spacing. To understand how these requirements are met, consider the frequency distributions of cloud-base mass fluxes from the WRF-CTL (25 km), WRF-CTL (8 km), and WRF-CPM (1 km) simulations, as shown in Figure 5b. The important point to note is all three have approximately log-Gaussian distribution, with the distribution shifting to the right with increasing resolution as expected. To meet the above requirements, the parameterized part of the cloud-base mass flux should make up for the differences between the WRF-CTL and the WRF-CPM results, and hence must be "scale aware." To that end, $\alpha(\Delta x)$ is set to

$$\alpha(\Delta x) = \beta \left(e^{\left(\frac{\Delta x - 1 km}{25 km - 1 km} \right)} - 1 \right) \qquad (7)$$

Under these assumptions, for an optimized constant value of β, comparisons of the total mass flux (the sum of resolved and parameterized cloud-base mass fluxes) from the WRF-LAMP and the WRF-CPM simulations are shown in Figure 5c. As desired, the resolution dependence of the total cloud-base mass flux is significantly reduced. As can be inferred from the equation, β and p, the stochasticity parameter discussed above, regulate the shift in the mean cloud-base mass flux and the total count of the distribution, respectively. Note that the total mass flux in LAMP is the sum of the resolved and parameterized convection; thus, the contribu-
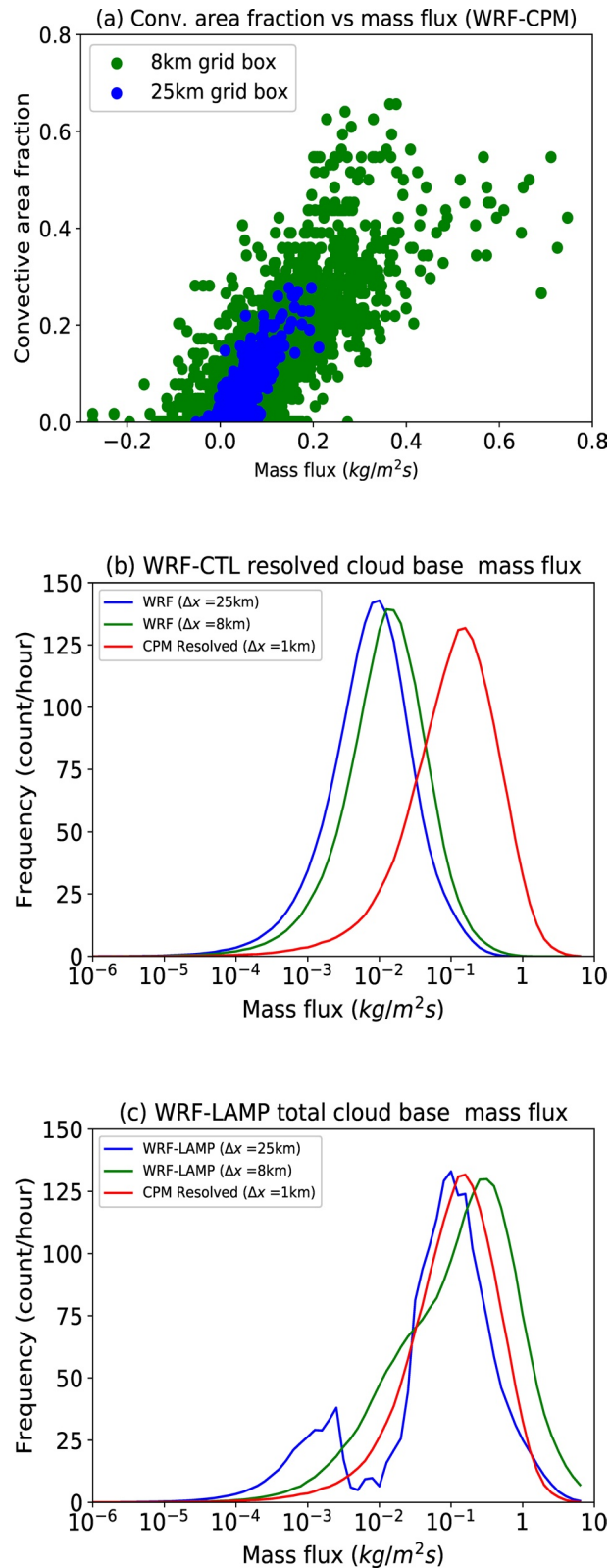
Figure 5. (a) The relationship between convective area fraction and average cloud-base mass flux over 25 and 8-km grid boxes obtained from WRF-CPM simulation, (b) comparison of the frequency distributions of resolved cloud-base mass flux from the WRF-CTL and WRF-CPM simulations, panel (c) as in panel (a), but for the total cloud-base mass-flux from the WRF-LAMP simulations.
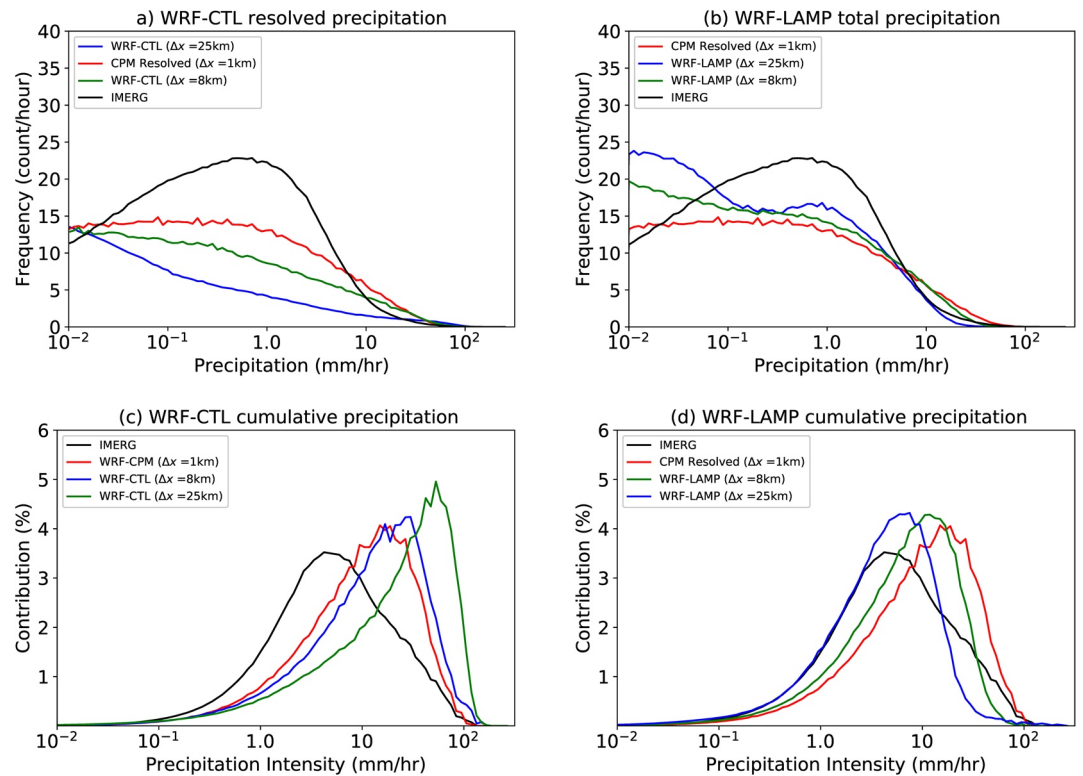
Figure 6. (a and b) Comparisons of frequency distribution of hourly precipitation from WRF-CTL and WRF-LAMP simulations with that from WRF-CPM and IMERG observations. Panels (c and d) like panels (a and b), but for the percentage contributions of the given precipitation intensity to the total.

tion of the smaller resolved mass flux is apparent in the secondary peak in the 25-km grid spacing at around 1.0×10^{-3} kg m^{-1} s^{-2}. While this is a limitation, as will be seen below, the impact of this secondary peak on precipitation statistics and mean precipitation is small. Once the new total convective area A_c is determined from Equation 6, the change ΔA_c is inferred by subtracting that of the previous time step. Then, using Equation 1, the change in the convective area within a given mass flux bin is determined. At this step, the requirement that $A_c = \sum_{i=1}^{n} c_i$ is enforced at every step by normalization. A subsample of mean cell size and the mean mass flux, determined using the given probability p, of the distribution (c) is passed as input to the entraining plume model (Appendix A) to calculate the heating and moistening tendencies associated with precipitation processes. p is a constant optimized to minimize the resolution sensitivity of the mass flux along with β. The number of nonzero bins would depend on the total convective area fraction. The entraining plume model is called for a given bin only if the randomly selected c_i is nonzero. The results for each subsampled bin are combined according to Equations 2–4 and provided to the host model. Before moving on to evaluation, we summarize the steps discussed above.

1. Based on the closure the total convective area is determined.
2. The distribution of the convective area c is updated.
3. A random subsample of the convective activity, determined by p, is assumed to have taken place within the given grid box and
4. That subsample is passed on to the entraining plume model.

Figure 6 provides a comparison of the resulting precipitation frequency distribution for WRF-LAMP with those for WRF-CTL and observations. The distribution represents the count of the number of grid points in one of 40 precipitation intensity bins in each hour. The mean values in the 40 bins increase exponentially from $10^{-2.0}$ to $10^{2.5}$ mm/hr. As the comparison between Figures 6a and 6b indicates, the WRF-LAMP produces precipitation statistics that are more in line with WRF-CPM (1 km) as well as IMERG and the sensitivity to grid-spacing is
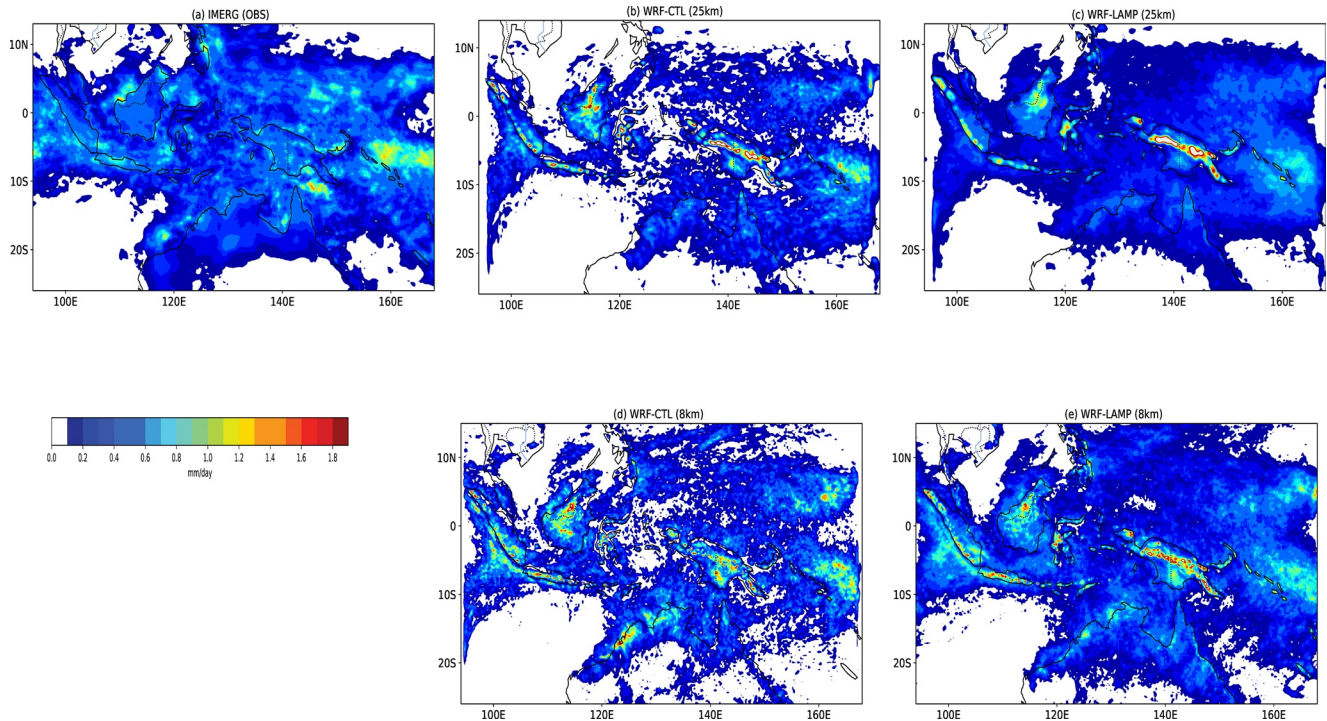
Figure 7. Two-month mean precipitation from (a) IMERG observations, (b and d) WRF-CTL and (c and e) WRF-LAMP simulations run at 25 and 8-km grid spacings.

much reduced. While beyond the scope of this study, the discrepancy between the precipitation statistics from the WRF-CPM simulation and the IMERG observation is worth noting. Ultimately the success of this approach to parameterization hinges on continued improvements in the training simulations or perhaps even preferably using actual observations for training, the latter is a subject of an ongoing work, which will be reported elsewhere. The percentage contributions of various precipitation intensities to the total are also calculated by multiplying the frequency with the corresponding precipitation intensity (Figures 6c and 6d). The convergence toward the observations of the WRF-LAMP simulations in comparison to WRF-CTL is apparent.

The spatial distribution of mean precipitation is also considered. Figure 7 shows comparisons of the 2-month mean precipitation from the WRF-CTL and WRF-LAMP simulations, along with IMERG observations. The WRF-CTL simulations typically underestimate the precipitation over the waters surrounding the Maritime Continent region and the WRF LAMP simulation appear to somewhat reduce that bias. Although these improvements are encouraging, they are direct results of the development of WRF-LAMP focused over the Australian monsoon region specifically. To assess the potential value of this approach to parameterization, its impacts on precipitation over other regimes must be examined. This is the subject of the next section.

3. Evaluation of Impact on Precipitation

The present evaluation is meant to assess the potential value of developing this approach toward a more mature parameterization for the coming generations of climate models. Thus, one must keep in mind that the development of the cloud population model has several steps each with room for improvement. For example, one can imagine an increased resolution and fidelity of the training simulation or preferably even using observational data for training. One could also improve on the plume model, the closure, etc. With that in mind, a comprehensive evaluation of the full parameterization against multiple suites of observations and other more mature parameterizations is left as a future work. In this section, we provide a comparatively preliminary documentation of the performance of LAMP under various environmental conditions. Specifically, we focus on precipitation statistics, the diurnal cycle over the global tropics and continental US, and the propagation of precipitation associated with MJO events. To that end, in addition to those already described in Section 2,
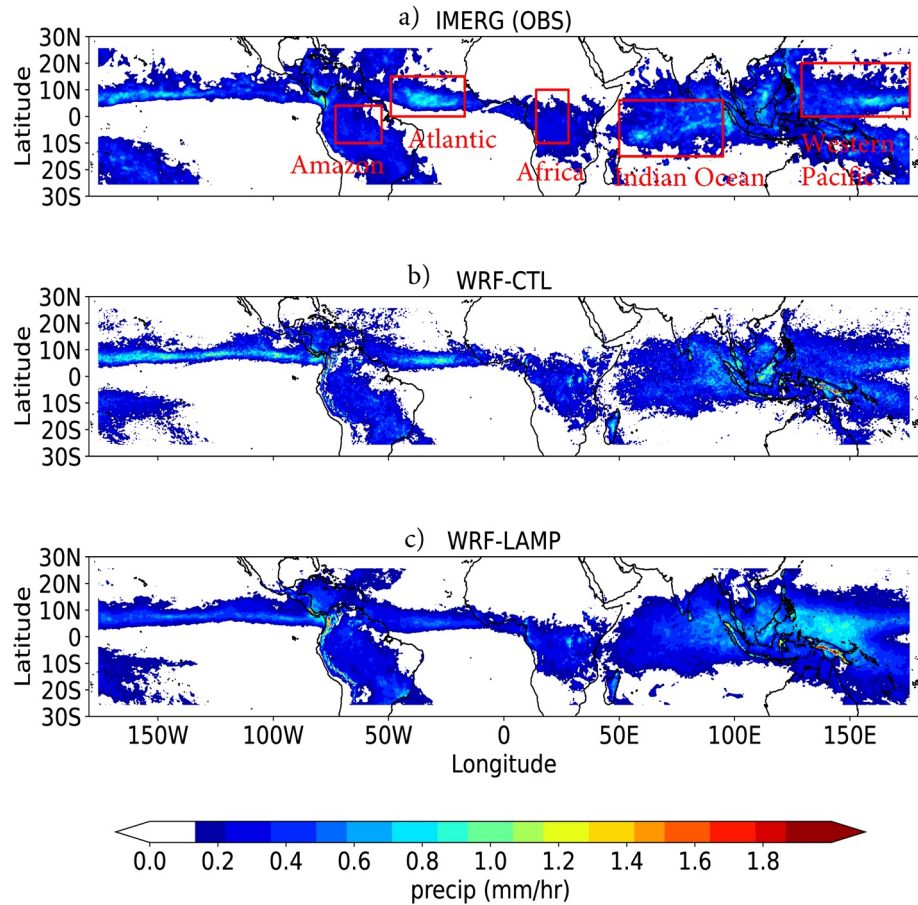
Figure 8. Three-month mean precipitation from (a) IMERG observations, (b) WRF-CTL, and (c) WRF-LAMP simulations over the tropical channel extending between 30°S and 30°N.

two additional pairs of simulations are performed. These simulations cover the tropical channel (hereafter TROPICS) and the continental US (hereafter CONUS) for periods of 1 October – 31 December 2011 (a period including a series of MJO events) and 1 April – 30 June 2016 (a rainy season with MCS-related precipitation), respectively. As for the Australian monsoon simulations discussed in Section 2, for the control cases (WRF-CTL, hereafter), the cumulus parameterization is turned off and in companion simulations, the LAMP parameterization is turned on (WRF-LAMP). All the evaluation simulations are run at a 25-km grid spacing. All other parameterizations, and the data sources used for lateral and surface conditions follow the Australian Monsoon development case discussed above.

Figure 8 shows the simulation domains and spatial distributions of the seasonal mean precipitation over the tropical channel (TROPICS) from the WRF-CTL and WRF-LAMP simulations compared with IMERG. While both simulations capture the main precipitation features (i.e., the ITCZ and continental precipitation over the various regions), WRF-LAMP has particularly high precipitation over the Western Pacific. This might be due to the oversensitivity of the cloud model to moisture rather than due to the neglect of evaporation of rain as the region is particularly moist. Figure 9 shows the spatial distribution of mean precipitation in the CONUS simulations compared to IMERG observations. Both the WRF-CTL and WRF-LAMP simulations capture the spatial distribution of precipitation well.

The model-simulated precipitation statistics over the five regions marked by the red boxes in Figure 8a, and over the CONUS region are calculated in a like manner to those shown in Figure 6, and they are compared with statistics from IMERG in Figure 10. The precipitation statistics in WRF-LAMP simulations (green) generally improve over the control to a varying degree, particularly for medium or high rain rates. In general, the underestimated
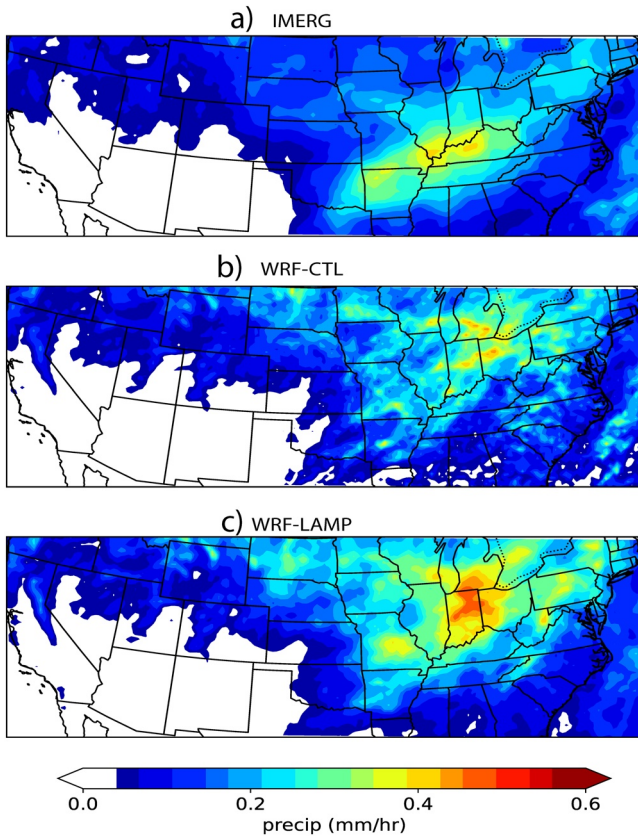
Figure 9. Three-month mean precipitation from (a) IMERG observation, (b) WRF-CTL and WRF-LAMP simulations run at the 25-km grid spacing over the continental US (CONUS).

frequencies of weak-to-moderate rain rates (0.1–10 mm/hr) in WRF-CTL are improved with LAMP. The frequencies of intense rain rates (>10 mm/hr) are generally reduced with WRF-LAMP compared to WRF-CTL, which is also mostly an improvement. Similar conclusions can also be drawn from the percentage contributions of various precipitation intensities (Figure 11). Specifically, over the land, the excessive amounts of rain produced by intense rain rates (>10 mm/hr) in WRF-CTL are reduced in WRF-LAMP, and the underestimated amounts from moderate rain rates (2–10 mm/hr) are also improved. While over the ocean, the reduction in the contribution from intense rain rates is excessive in LAMP, but the improvements in low and moderate rain rates are nonetheless apparent.

The diurnal cycles over these regions are represented well in both the WRF-CTL and WRF-LAMP simulations (Figure 12). Although many simulations with explicit convection are known to be able to produce reasonable representations of the diurnal cycle (e.g., Keat et al., 2019; Marsham et al., 2013), by contrast, many simulations with the parameterized convection struggle to produce good results (C. Zhang et al., 2020; Dirmeyer et al., 2012), despite some recent improvements (e.g., Baba, 2020; Bechtold et al., 2014; Xie et al., 2019). There is a bias of excess precipitation over the western Pacific with WRF-LAMP (Figure 12f). This excess precipitation over the western Pacific indicates that the convective activity in WRF-LAMP is overly sensitive to moisture, which may be related to the choice of entrainment rate in the entraining plume model. The relatively good diurnal cycle arises from the treatment of the WRF-LAMP closure, in that a convective area fraction is set to be proportional to the resolved cloud-base mass flux, as compared to many common closures that link the parameterized convection to measures of instability that peak at noon.

Finally, the propagation of MJO precipitation signals in WRF simulations is examined using MJO events observed in the winter of 2011. Figure 13 shows the Hovmöller diagrams of precipitation averaged between 5°S and 5°N, and the eastward propagation of the precipitation signals associated with three MJO events is most apparent in IMERG and in WRF-LAMP. As is common in many traditional parameterizations, the control simulation has a persistent precipitation signal during an otherwise suppressed phase of the MJO (S. M. Hagos et al., 2016). WRF-LAMP reduces the contribution of the low-intensity precipitation that prevails in WRF-CTL during the suppressed phases of the MJO resulting in a better agreement with the observations. This contrasts with many quasi equilibrium-based cumulus parameterizations that typically degrade the propagation of precipitation signals (e.g., Jiang, 2017).

While this study demonstrates the utility of machine-learning-assisted stochastic cloud population model for parameterization, the actual application in a global modeling research and operation would require addressing a few issues. The first issue is related to the imperfection of the training data. This has two aspects. The first one is related to biases in the convection-permitting model simulation used for training. One possible way to address this is training the algorithms directly using observations such as data from radar scans and soundings. Granted such observations have their own limitations. The second is generalizability in the sense of regional dependence of the relationship captured by the machine learning algorithm. Ideally, such a training would sample all major regions of the convective activity, which in theory could be obtained from global convection permitting model simulations like those from DYAMOND (Stevens et al., 2019) as discussed in Section 2.4. The third issue is related to closure. In this work, we argue that the resolved cloud-base mass flux contains information about a subgrid convective activity that could be exploited for closure. This is like moisture-convergence-based (Kuo, 1974) closures because the resolved mass flux at cloud base and the height of cloud base define the mass convergence while the effect of moisture is implicit in the height of the cloud base. This approach, while it has distinct advantages in that its accuracy improves with increasing resolution and scale-awareness can be introduced in a straightforward manner, could introduce large errors at courser resolutions as scale separation is
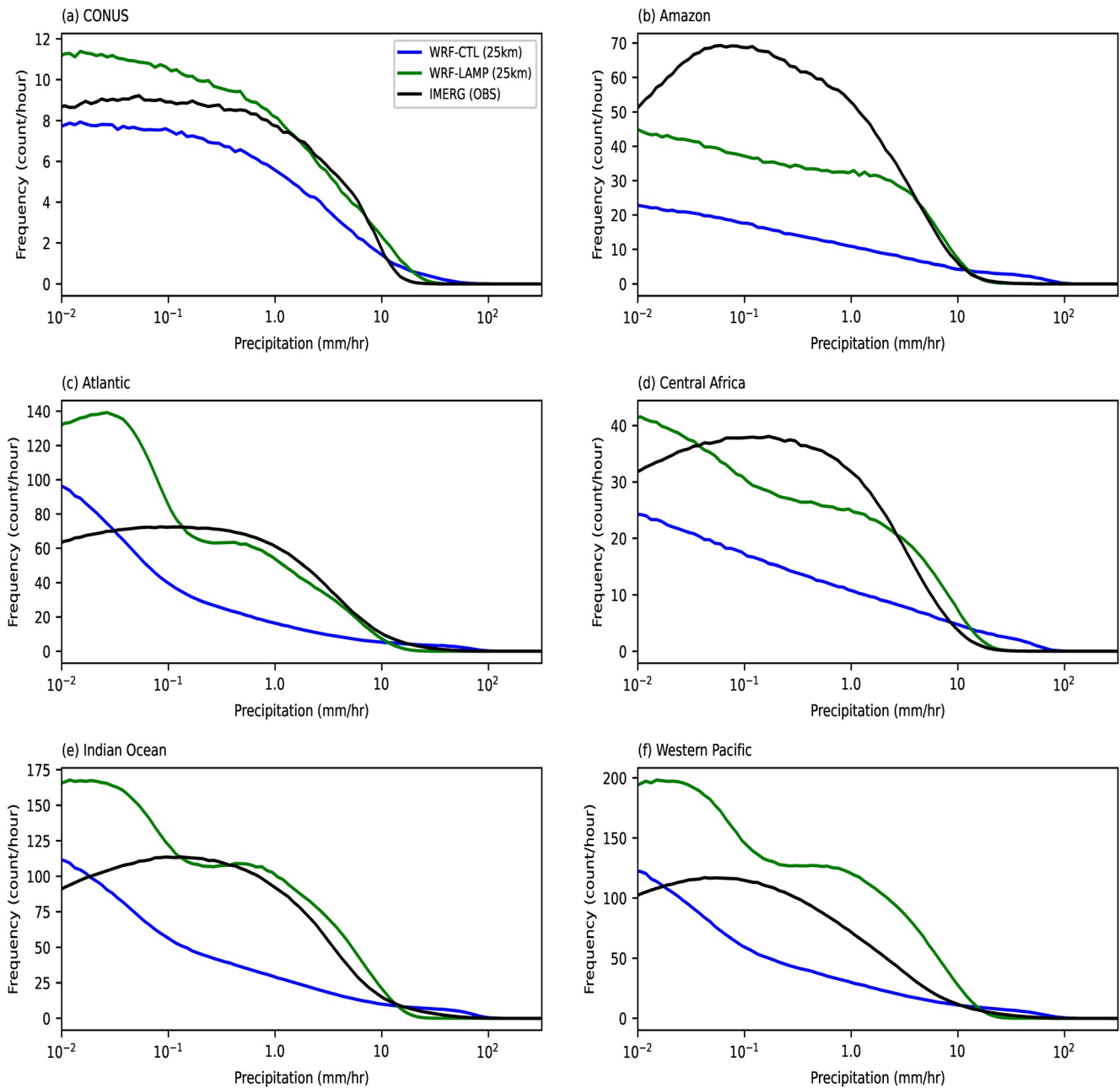
Figure 10. Comparisons of frequency distribution of precipitation from the WRF-CTL and WRF-LAMP simulations with that from IMERG observations over the regions marked by the red boxes in Figure 8 and the continental US. All the hourly precipitation data from the simulations and observations are on the 25-km grid spacing.

the main rationale for parameterization in the first place. The fourth issue is related to the cloud model, which ultimately calculates the thermodynamic tendencies based on the predicted cloud-base mass flux and the environment. An obvious limitation of the cloud model presented here is a lack of representation of evaporation of precipitation, which can potentially lead to excessive precipitation over regions with dry boundary layers. For more practical applications, coupling a complex cloud model that accounts for this and other processes would be necessary.
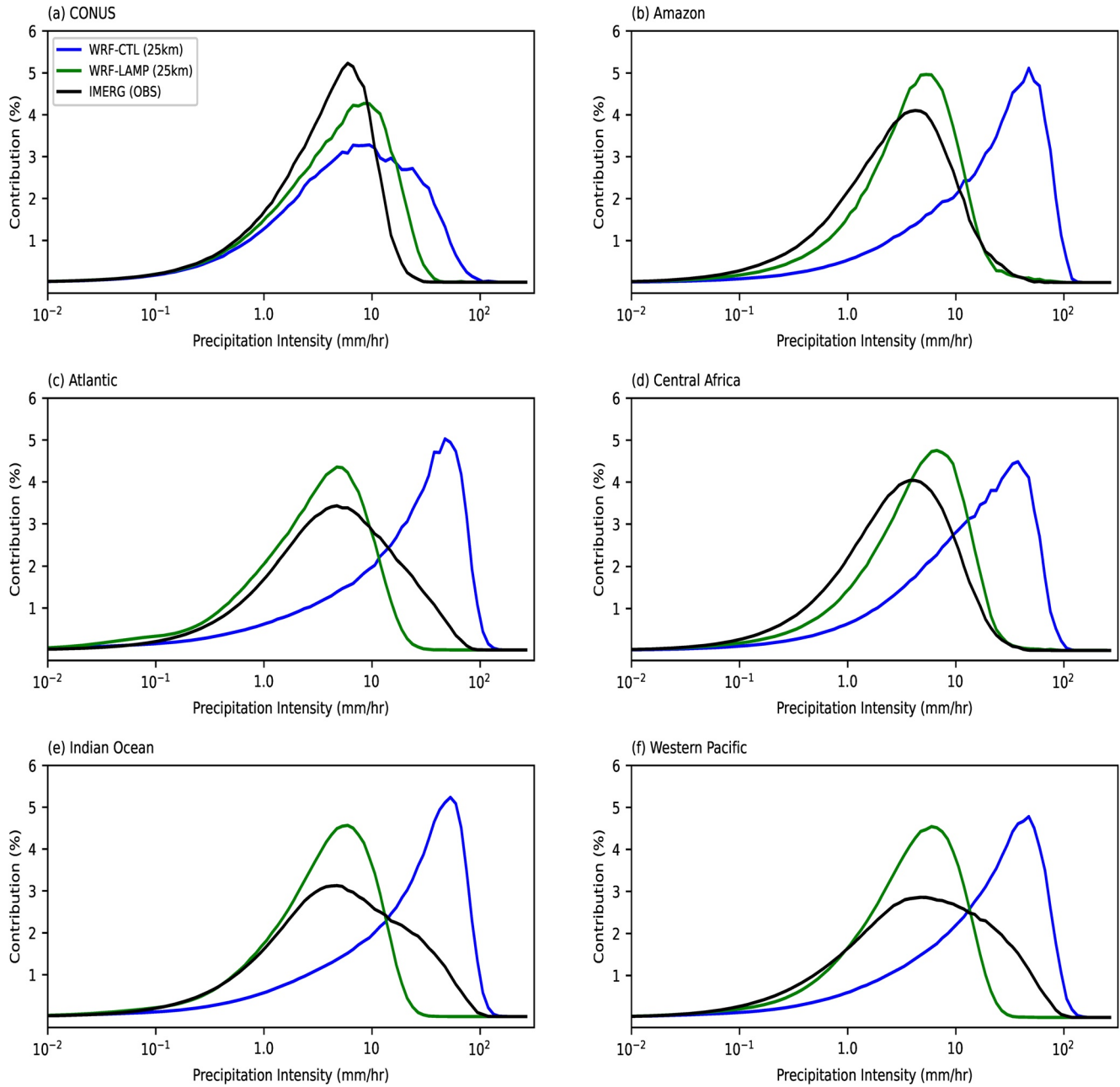
Figure 11. Comparisons of percentage contributions of precipitation intensities from the WRF-CTL and WRF-LAMP simulations with that from IMERG observations over the regions marked by the red boxes in Figure 8 and over the continental US. All the hourly precipitation data from all the simulations and observations are on the 25-km grid spacing.

4. Discussion

Increased availability of computational resources is enabling climate model simulations of the order of 10s of kilometers of the grid spacing. These advances require rethinking the role and design of cumulus parameterizations since the use of traditional cumulus parameterizations developed for coarser grid spacings has been widely documented to contribute to biases in precipitation statistics as well as issues in simulating modes of variability such as the diurnal cycle, the propagation of the MJO, and associated tropical precipitation signals. Convection-resolving models of order km grid spacing have shown some successes in eliminating or reducing these
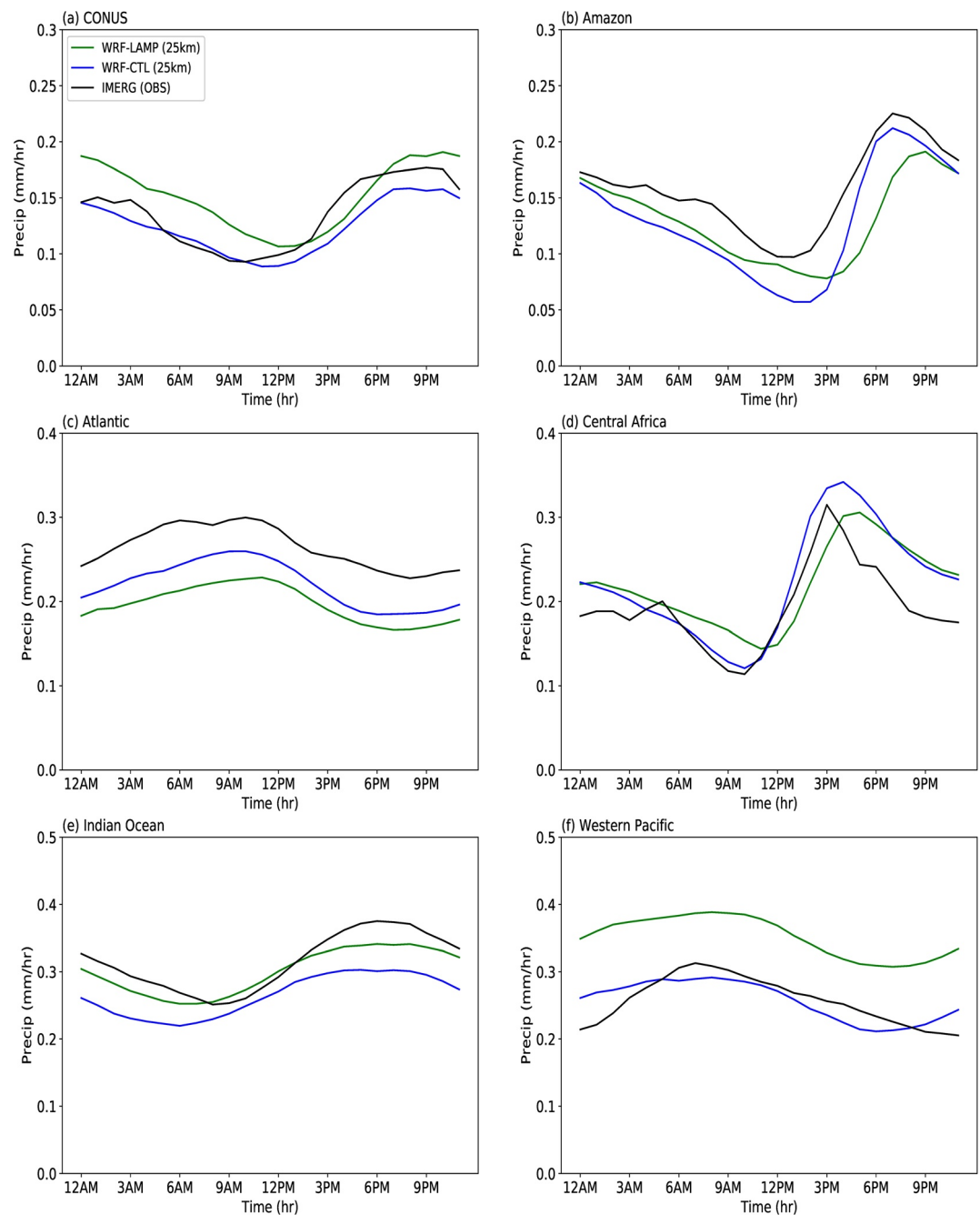
Figure 12. The mean diurnal cycles of precipitation from the WRF-CTL and WRF-LAMP simulations with that from IMERG observations over the six regions marked by the red boxes in Figure 8 and the continental US.

biases. The present study contributes to the development of parameterizations for grid spacings between 25 and 1 km by exploiting high-resolution limited-area modeling and machine learning.

The WRF-LAMP parameterization aims to represent variability in the cloud-base mass flux that is associated with lifecycles of clouds and interactions among them using a cloud population model with a machine-learning derived transition function. Given the change in the total convective area in a grid box, the population model predicts a distribution of convective areas for given bins of the cloud-base mass flux and cell size statistics. As a closure, the total convective area in a grid box is assumed to be proportional to the resolved cloud-base mass flux obtained from the host model, WRF. Cloud-base mass fluxes and cell sizes are drawn randomly as a subset of the
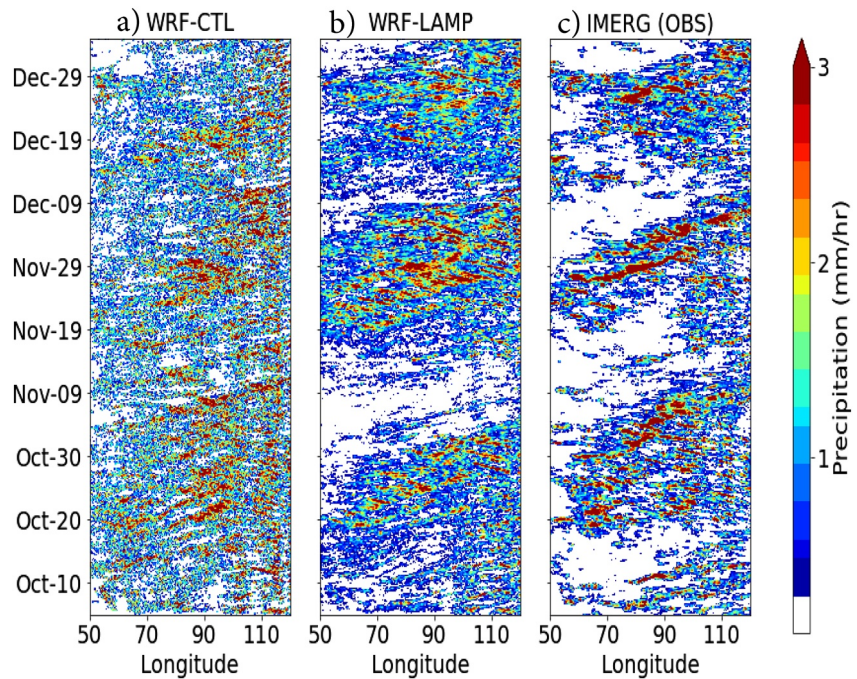
Figure 13. Hovmöller diagram of propagation of precipitation associated with MJO events from the WRF-CTL and WRF-LAMP simulations compared with IMERG observations during winter of 2011. All are averaged between 5°N and 5°S.

predicted distribution and these are then fed to an entraining plume model that calculates heating and moistening tendencies as well as precipitation. The tendencies from each bin are combined and fed back to the host model.

The model performance is evaluated in terms of precipitation statistics, the diurnal cycle, the precipitation climatology (over tropical and midlatitude regions), and the propagation of precipitation signals associated with the MJO. Precipitation statistics in coupled cloud-population-model simulations are significantly improved over those in control simulations with no cumulus parameterization over many regions. It is also shown that the proposed parameterization represents well the diurnal cycle over both land and ocean regions in the tropics and over the continental US. This is attributed to the closure that relates the subgrid convective area to the resolved-scale cloud-base mass flux. This key assumption is based on the arbitrariness of the model grid-spacing and the need to do away with the "large-scale" and "convective-scale" separation. Similarly, unlike traditional quasi equilibrium-based parameterizations, it improves the propagation of precipitation signals associated with the MJO by reducing excessive precipitation during suppressed phases.

It should be noted that the parameterization approach proposed here is in some ways similar to other stochastic representations of the convection. But unlike many approaches that prescribe the distribution from which the convective events are drawn, the cloud population model here predicts the distribution based on the machine-learning-trained transition function. As such it has limitations that follow from the specificity of the training simulation, as is apparent, for example, in the wet bias over the western Pacific. Moreover, as a simple demonstration of the approach, several simplifying assumptions are made. Thus, the present study has to be considered as a step toward a more general class of approaches utilizing observations, high-resolution model simulations, and machine learning toward efficient representation of the convection in the next generation of global models. Some potential benefits from following this parameterization approach have been demonstrated in comparison to control simulations without a parameterization. Future work will include an examination of the performance of this approach in comparison to other approaches with comparable levels of complexity, of the scope for tuning as well as more extensive evaluations against observations from multiple platforms. Assessment of global applicability of transition functions obtained from a given set of observations or model simulations is also of scientific interest as it can reveal previously unknown cloud transition processes specific to a regime.

Appendix A: Entraining Plume Model

As in many mass-flux-based cumulus parameterizations, WRF-LAMP relies on an entraining plume model to calculate moistening and heating tendencies for the host model as well as the associated precipitation. In addition to the thermodynamic profile, the WRF-LAMP entraining plume model is provided with the subsample cloud-base mass fluxes $\mathbf{m_{cb}}$ and the corresponding subsample cell sizes $\boldsymbol{a}$. In this appendix, a description of the plume model is provided. It is based on that developed by Kim and Kang (2012) but with several differences detailed below.

The equations governing the updraft mass flux (M_u) and conserved scalar quantities ϕ_u are given by

$$\frac{d M_u}{d z} = (\lambda_i - \delta_i)\, M_u \tag{A1}$$

$$\frac{d \phi_u}{d z} = -\lambda_i\, (\phi_u - \phi_e) + S_{\phi u} \tag{A2}$$

where λ_i and δ_i are the fractional entrainment and detrainment rates, respectively, and $S_{\phi u}$ is a possible source term. ϕ_u is the updraft value of a scalar variable, including the total water mixing ratio (qt) and the liquid water potential temperature, the latter being given by

$$\theta_l = T \left(\frac{p_s}{p} \right)^k \left(1 - \frac{L_v q_l}{c_{pd} T} \right) \tag{A3}$$

where T is the temperature, ps and p are the pressure at the surface and at the given layer, respectively, and ql is the liquid water mixing ratio.

Buoyancy is defined by the difference in the virtual potential temperature between the updraft parcel (subscript u) and the environment (subscript e) as

$$B_u = g\, (\theta v_u - \theta v_e)\, / \theta v_e - g q_{lu} \tag{A4}$$

where

$$\theta_v = T \left(\frac{p_s}{p} \right)^k (1 + 0.608 q_v - q_l - q_i) \tag{A5}$$

For the height levels between cloud base z_{cb} and the level of neutral buoyancy z_{nb} (where $B_u = 0.0$) and consistent with many other studies (e.g., Neggers, 2015; Wagner & Graf, 2010; Stirling & Stratton, 2012; and references therein), the entrainment rate is assumed to be inversely proportional to the convective cell radius. Furthermore, it is assumed to be inversely proportional with height, as is often assumed while the detrainment rate is assumed to be zero.

$$\lambda_i = \lambda_{max} \left(\frac{a_1}{a_i} \right)^{0.5} \left(\frac{z_{cb}}{z} \right) \tag{A6}$$

Above the level of neutral buoyancy, the detrainment rate is set to be

$$\delta_i = \delta_{max} \left(\frac{a_1}{a_i} \right)^{0.5} \left(\frac{z_{cb}}{z} \right) \tag{A7}$$

and δ_{max} is assumed to be equal to λ_{max}. This treatment of detrainment corresponds to an assumption that the detrainment in a bulk parameterization is dominated by the termination of plumes within the underlying cloud spectrum as opposed to the mixing detrainment at the edges of individual clouds (Derbyshire et al., 2011; Plant, 2010).

As the entraining plume rises from one level to the next, starting at cloud base, it entrains environmental air according to Equation A1. The cloud water is calculated at each level as

$$q_{lu} = \max\, (q_{vu} - q_{v,sat}, 0) \tag{A8}$$

where the saturation mixing ratio in the updraft is approximated using the Clausius-Clapeyron equation

$$q_{v,\text{sat}} = \frac{q_{v0}p_0}{p} \exp\left(-\frac{L_v}{R_v}\left(\frac{1}{T_u} - \frac{1}{T_0}\right)\right) \tag{A9}$$

with the parcel temperature being given by

$$T_u = \theta_u \left(\frac{p}{p_s}\right)^{\kappa} \tag{A10}$$

and q_{v0} is a reference value of the saturation water vapor mixing ratio at the given reference temperature and pressure, T_0 and p_0. Following Lord (1982) and G. J. Zhang and McFarlane (1995), the production of rain at a given level is assumed to be proportional to the vertical flux of cloud water in the updraft as

$$R_r = c_0 q_{lu} M_u \tag{A11}$$

where c_0 is a cloud to the rainwater autoconversion parameter. Above freezing level, the fraction of q_{lu} that is converted to ice (q_{iu}) is assumed to increase linearly with the decreasing parcel temperature.

$$q_{iu} = q_{lu}\max\left(\frac{(T_u - T_f)}{(T_{min} - T_f)}, 0\right) \tag{A12}$$

where T_f is the freezing temperature and $T_{\min}$ is a given minimum temperature. Once the condensation and freezing have taken place, the θ_{vu} and q_{vu} are updated.

$$\theta_{vu} \rightarrow \theta_{vu} + \frac{\theta_v}{c_p T_u}(L_v q_{lu} + L_f q_{iu}) \tag{A13}$$

$$q_{vu} \rightarrow q_{v,sat} \tag{A14}$$

The buoyancy is then updated and the plume calculations integrated up to the next model level until the model top is reached.

The precipitation is obtained from summing the rain production from the top of the atmosphere (z_t) to the cloud base (z_{cb}). The evaporation of rain is neglected in this simple model. But one can incorporate such evaporation, on its dependence and effect on precipitation and relative humidity (Gregory, 1995)

Table A1
Parameters for the Entraining Plume Model

Parameter	Value
c_0	1.0e−4/m
c_e	2.0e−3
R	287.05 J/(kg·K)
R_v	461.61 J/(kg·K)
L_v	2.5e6 KJ/Kg
L_f	3.35e5 J/Kg
K	0.622
p_0	90,000.0 Pa
c_p	1,005.0 J/(kg·K)
T_0	288.15 K
T_{max}	263.15 K
T_{min}	233.15 K
q_{v0}	0.006 kg/kg
λ_{max}	0.001/m

$$P_{cu} == \int_{z_{cb}}^{z_t} R_r(x)\, dx \tag{A15}$$

Finally, the tendencies of the total water mixing ratio and the liquid water potential temperature associated with the rain are calculated as follows.

$$\left.\frac{dq_t}{dt}\right|_{\text{rain}} = -R_r \tag{A16}$$

$$\left.\frac{d\theta_l}{dt}\right|_{\text{rain}} = \left(\frac{L_v \theta_{le}}{c_p T_e}\right) R_r \tag{A17}$$

Table A1 shows the constants and parameter choices in the entraining plume model.

Data Availability Statement

The WRF-LAMP model and analysis codes and data are available at https://portal.nersc.gov/project/cpmmjo/WRF-LAMP/.

References

Arakawa, A., & Schubert, W. H. (1974). Interaction of a cumulus cloud ensemble with the large-scale environment, Part I. *Journal of the Atmospheric Sciences*, *31*, 674–701. https://doi.org/10.1175/1520-0469(1974)031<0674:ioacce>2.0.co;2

Arakawa, A., & Wu, C.-M. (2013). A unified representation of deep moist convection in numerical modeling of the atmosphere. Part I. *Journal of the Atmospheric Sciences*, *70*, 1977–1992. https://doi.org/10.1175/jas-d-12-0330.1

Baba, Y. (2020). Diurnal cycle of precipitation over the Maritime Continent simulated by a spectral cumulus parameterization. *Dynamics of Atmospheres and Oceans*, *91*, 101160. https://doi.org/10.1016/j.dynatmoce.2020.101160

Bechtold, P., Semane, N., Lopez, P., Chaboureau, J., Beljaars, A., & Bormann, N. (2014). Representing equilibrium and nonequilibrium convection in large-scale models. *Journal of the Atmospheric Sciences*, *71*, 734–753. https://doi.org/10.1175/jas-d-13-0163.1

Bryan, G. H., Wyngaard, J. C., & Fritsch, J. M. (2003). Resolution requirements for the simulation of deep moist convection. *Monthly Weather Review*, *131*(10), 2394–2416. https://doi.org/10.1175/1520-0493(2003)131<2394:rrftso>2.0.co;2

Clark, P., Roberts, N., Lean, H., Ballard, S. P., & Charlton-Perez, C. (2016). Convection-permitting models: A step-change in rainfall forecasting. *Meteorological Applications*, *23*, 165–181. https://doi.org/10.1002/met.1538

Copernicus Climate Change Service (C3S) (2017). ERA5: Fifth generation of ECMWF atmospheric reanalyses of the global climate. Copernicus Climate Change Service Climate Data Store (CDS). Retrieved from https://cds.climate.copernicus.eu/#!/home

Cui, W., Dong, X., Xi, B., Feng, Z., & Fan, J. (2020). Can the GPM IMERG final product accurately represent MCSs' precipitation characteristics over the central and eastern United States? *Journal of Hydrometeorology*, *21*(1), 39–57. https://doi.org/10.1175/jhm-d-19-0123.1

Davini, P., von Hardenberg, J., Corti, S., Christensen, H. M., Juricke, S., Subramanian, A., et al. (2017). Climate SPHINX: Evaluating the impact of resolution and stochastic physics parameterisations in the EC-Earth global climate model. *Geoscientific Model Development*, *10*, 1383–1402. https://doi.org/10.5194/gmd-10-1383-2017

Derbyshire, S. H., Maidens, A. V., Milton, S. F., Stratton, R. A., & Willett, M. R. (2011). Adaptive detrainment in a convective parametrization. *Quarterly Journal of the Royal Meteorological Society*, *137*, 1856–1871. https://doi.org/10.1002/qj.875

Dezfuli, A. K., Ichoku, C. M., Huffman, G. J., Mohr, K. I., Selker, J. S., van de Giesen, N., et al. (2017). Validation of IMERG precipitation in Africa. *Journal of Hydrometeorology*, *18*(10), 2817–2825.

Dirmeyer, P. A., Cash, B. A., Kinter, J. L., III, Jung, T., Marx, L., Satoh, M., et al. (2012). Simulating the diurnal cycle of rainfall in global climate models: Resolution versus parameterization. *Climate Dynamics*, *39*, 399–418. https://doi.org/10.1007/s00382-011-1127-9

Ek, M. B., Mitchell, K. E., Lin, Y., Rogers, E., Grumman, P., Koren, V., et al. (2003). Implementation of Noah land surface model advances in the National Centers for environmental prediction operational mesoscale Eta model. *Journal of Geophysical Research*, *108*, 8851. https://doi.org/10.1175/jhm-d-17-0139.1

Emanuel, K. A. (1994). *Atmospheric convection*. Oxford University Press.

Feng, Z., Leung, L. R., Liu, N., Wang, J., Houze, R. A., Li, J., et al. (2021). A global high-resolution mesoscale convective system database using satellite-derived cloud tops, surface precipitation, and tracking. *Journal of Geophysical Research: Atmospheres*, *126*, e2020JD034202. https://doi.org/10.1029/2020JD034202

Gerard, L. (2015). Bulk mass-flux perturbation formulation for a unified approach of deep convection at high resolution. *Monthly Weather Review*, *143*, 4038–4063. https://doi.org/10.1175/mwr-d-15-0030.1

Gingrey, A., Varble, A., & Zipser, E. (2018). Relationships between extreme rain rates and convective intensities from the perspectives of TRMM and WSR-88D radars. *Journal of Applied Meteorology and Climatology*, *57*(6), 1353–1369. https://doi.org/10.1175/jamc-d-17-0240.1

Goswami, B. B., Khouider, B., Phani, R., Mukhopadhyay, P., & Majda, A. J. (2017). Implementation and calibration of a stochastic multicloud convective parameterization in the NCEP Climate Forecast System (CFSv2). *Journal of Advances in Modeling Earth Systems*, *9*, 1721–1739. https://doi.org/10.1002/2017MS001014

Gregory, D. (1995). A consistent treatment of the evaporation of rain and snow for use in large-scale models. *Monthly Weather Review*, *123*(9), 2716–2732. https://doi.org/10.1175/1520-0493(1995)123<2716:actote>2.0.co;2

Hagos, S., Feng, Z., Burleyson, C. D., Lim, K.-S. S., Wu, D., & Thompson, G. (2014). Evaluation of convection-permitting model simulations of cloud populations associated with the Madden-Julian Oscillation using data collected during the AMIE/DYNAMO field campaign. *Journal of Geophysical Research: Atmospheres*, *119*, 12052–12068. https://doi.org/10.1002/2014jd022143

Hagos, S., Feng, Z., Plant, R. S., Houze, R. A., & Xiao, H. (2018). A stochastic framework for modeling the population dynamics of convective clouds. *Journal of Advances in Modeling Earth Systems*, *10*, 448–465. https://doi.org/10.1002/2017MS001214

Hagos, S., Feng, Z., Plant, R. S., & Protat, A. (2020). A machine learning assisted development of a model for the populations of convective and stratiform clouds. *Journal of Advances in Modeling Earth Systems*, *12*, e2019MS001798. https://doi.org/10.1029/2019ms001798

Hagos, S. M., Feng, Z., Burleyson, C. D., Zhao, C., Martini, M. N., & Berg, L. K. (2016). Moist process biases in simulations of the Madden–Julian oscillation episodes observed during the AMIE/DYNAMO field campaign. *Journal of Climate*, *29*(3), 1091–1107. https://doi.org/10.1175/jcli-d-15-0349.1

Heinze, R., Dipankar, A., Henken, C. C., Moseley, C., Sourdeval, O., Trömel, S., et al. (2017). Large-eddy simulations over Germany using ICON: A comprehensive evaluation. *Quarterly Journal of the Royal Meteorological Society*, *143*, 69–100. https://doi.org/10.1002/qj.2947

Hong, S.-Y., Noh, Y., & Dudhia, J. (2006). A new vertical diffusion package with an explicit treatment of entrainment processes. *Monthly Weather Review*, *134*, 2318–2341. https://doi.org/10.1175/mwr3199.1

Huffman, G. J., Bolvin, D. T., Nelkin, E. J., & Tan, J. (2019). *Integrated Multi-satellitE Retrievals for GPM (IMERG) technical documentation* (Technical documentation, p. 77). Retrieved from https://pmm.nasa.gov/sites/default/files/document_files/IMERG_doc_190909.pdf

Islam, M. A., Yu, B., & Cartwright, N. (2020). Assessment and comparison of five satellite precipitation products in Australia. *Journal of Hydrology*, *590*, 125474. https://doi.org/10.1016/j.jhydrol.2020.125474

Jiang, X. (2017). Key processes for the eastward propagation of the Madden-Julian Oscillation based on multimodel simulations. *Journal of Geophysical Research: Atmospheres*, *122*, 755–770. https://doi.org/10.1002/2016JD025955

Janjic, Z. I. (2001). Nonsingular implementation of the Mellor-Yamada level 2.5 scheme in the NCEP Meso model. *NOAA/NWS/NCEP Office Note*, *437*, 61.

Jones, T. R., & Randall, D. A. (2011). Quantifying the limits of convective parameterizations. *Journal of Geophysical Research*, *116*, D08210. https://doi.org/10.1029/2010JD014913

Keat, W. J., Stein, T. H. M., Phaduli, E., Landman, S., Becker, E., Bopape, M. J. M., et al. (2019). Convective initiation and storm life cycles in -convection permitting simulations of the Met Office Unified-Model over South Africa. *Quarterly Journal of the Royal Meteorological Society*, *145*, 1323–1336. https://doi.org/10.1002/qj.3487

Khouider, B., Biello, J., & Majda, A. (2010). A stochastic multicloud model for tropical convection. *Communications in Mathematical Sciences*, *8*(1), 187–216.

Khouider, B., Majda, A. J., & Katsoulakis, M. A. (2003). Coarse-grained stochastic models for tropical convection and climate. *Proceedings of the National Academy of Sciences*, *100*, 11941–11946. https://doi.org/10.1073/pnas.1634951100

Kim, D., & Kang, I.-S. (2012). A bulk mass flux convection scheme for a climate model – Description and moisture sensitivity. *Climate Dynamics*, *38*, 411–429. https://doi.org/10.1007/s00382-010-0972-2

Kingma, D. P., & Ba, J. (2015). Adam: A Method for Stochastic Optimization. *International Conference on Learning Representations 2015*. https://arxiv.org/abs/1412.6980

Kuo, H. L. (1974). Further studies of the parameterization of the influence of cumulus convection on large-scale flow. *Journal of the Atmospheric Sciences*, *31*(5), 1232–1240. https://doi.org/10.1175/1520-0469(1974)031<1232:fsotpo>2.0.co;2

Lord, S. J. (1982). Interaction of a cumulus cloud ensemble with the large-scale environment. Part III: Semi-prognostic test of the Arakawa-Schubert cumulus parameterization. *Journal of the Atmospheric Sciences*, *39*, 88–103. https://doi.org/10.1175/1520-0469(1982)039<0088:ioacce>2.0.co;2

Majda, A. J., & Khouider, B. (2002). Stochastic and mesoscopic models for tropical convection. *Proceedings of the National Academy of Sciences*, *99*, 1123–1128. https://doi.org/10.1073/pnas.032663199

Maranan, M., Fink, A. H., Knippertz, P., Amekudzi, L. K., Atiah, W. A., & Stengel, M. (2020). A process-based validation of GPM IMERG and its sources using a mesoscale rain gauge network in the West African forest zone. *Journal of Hydrometeorology*, *21*(4), 729–749. https://doi.org/10.1175/jhm-d-19-0257.1

Marsham, J. H., Dixon, N., Garcia-Carreras, L., Lister, G. M. S., Parker, D. J., Knippertz, P., & Birch, C. (2013). The role of moist convection in the West African monsoon system—Insights from continental-scale convection-permitting simulations. *Geophysical Research Letters*, *40*, 1843–1849. https://doi.org/10.1002/grl.50347

Mlawer, E. J., Taubman, S. J., Brown, P. D., Iacono, M. J., & Clough, S. A. (1997). Radiative transfer for inhomogeneous atmospheres: RRTM, a validated correlated-k model for the longwave. *Journal of Geophysical Research*, *102*(D14), 16663–16682. https://doi.org/10.1029/97jd00237

Morcrette, J., Barker, H. W., Cole, J. N., Iacono, M. J., & Pincus, R. (2008). Impact of a new radiation package, McRad, in the ECMWF integrated forecasting system: Impact of a new package, radiation package, McRad, in the ECMWF integrated forecasting system. *Monthly Weather Review*, *136*, 4773–4798. https://doi.org/10.1175/2008mwr2363.1

Murali Krishna, U. V., Das, S. K., Deshpande, S. M., Doiphode, S. L., & Pandithurai, G. (2017). The assessment of Global Precipitation Measurement estimates over the Indian subcontinent. *Earth and Space Science*, *4*, 540–553. https://doi.org/10.1002/2017EA000285

Neggers, R. A. J. (2015). Exploring bin-macrophysics models for moist convective transport and clouds. *Journal of Advances in Modeling Earth Systems*, *7*, 2079–2104. https://doi.org/10.1002/2015MS000502

Plant, R. S. (2010). A review of the theoretical basis for bulk mass flux convective parameterization. *Atmospheric Chemistry and Physics*, *10*, 3529–3544. https://doi.org/10.5194/acp-10-3529-2010

Plant, R. S., & Craig, G. C. (2008). A stochastic parameterization for deep convection based on equilibrium statistics. *Journal of the Atmospheric Sciences*, *65*, 87–105. https://doi.org/10.1175/2007JAS2263.1

Poujol, B., Prein, A. F., & Newman, A. J. (2020). Kilometer-scale modeling projects a tripling of Alaskan convective storms in future climate. *Climate Dynamics*, *55*, 3543–3564. https://doi.org/10.1007/s00382-020-05466-1

Rio, C., Del Genio, A. D., & Hourdin, F. (2019). Ongoing breakthroughs in convective parameterization. *Current Climate Change Reports*, *5*(2), 95–111. https://doi.org/10.1007/s40641-019-00127-w

Skamarock, W. C., Klemp, J. B., Dudhia, J., Gill, D. O., Barker, D. M., Duda, M. G., et al. (2008). *A description of the advanced research WRF version 3* (NCAR Technical Note, NCAR/TN-475 + STR). Mesoscale and Microscale Meteorology Division, National Center for Atmospheric Research.

Stevens, B., Satoh, M., Auger, L., Biercamp, J., Bretherton, C. S., Chen, X., et al. (2019). DYAMOND: The DYnamics of the atmospheric general circulation modeled on non-hydrostatic domains. *Progress in Earth and Planetary Science*, *6*, 61. https://doi.org/10.1186/s40645-019-0304-z

Stirling, J., & Stratton, R. A. (2012). Entrainment processes in the diurnal cycle of deep convection over land. *Quarterly Journal of the Royal Meteorological Society*, *138*, 1135–1149. https://doi.org/10.1002/qj.1868

Teixeira, J., & Reynolds, C. A. (2008). Stochastic nature of physical parameterizations in ensemble prediction: A stochastic convection approach. *Monthly Weather Review*, *136*, 483–496. https://doi.org/10.1175/2007mwr1870.1

Thompson, G., Field, P. R., Rasmussen, R. M., & Hall, W. D. (2008). Explicit forecasts of winter precipitation using an improved bulk microphysics scheme. Part II: Implementation of a new snow parameterization. *Monthly Weather Review*, *136*, 5095–5115. https://doi.org/10.1175/2008mwr2387.1

Wagner, T. M., & Graf, H.-F. (2010). An ensemble cumulus convection parameterization with explicit cloud treatment. *Journal of the Atmospheric Sciences*, *67*, 3854–3869. https://doi.org/10.1175/2010JAS3485.1

Wang, Y., Zhang, G. J., & Craig, G. C. (2016). Stochastic convective parameterization improving the simulation of tropical precipitation variability in the NCAR CAM5. *Geophysical Research Letters*, *43*, 6612–6619. https://doi.org/10.1002/2016GL069818

Wang, Y., Zhang, G. J., Xie, S., Lin, W., Craig, G. C., Tang, Q., & Ma, H.-Y. (2021). Effects of coupling a stochastic convective parameterization with the Zhang–McFarlane scheme on precipitation simulation in the DOE E3SMv1.0 atmosphere model. *Geoscientific Model Development*, *14*, 1575–1593. https://doi.org/10.5194/gmd-14-1575-2021

Xie, S., Wang, Y.-C., Lin, W., Ma, H.-Y., Tang, Q., Tang, S., et al. (2019). Improved diurnal cycle of precipitation in E3SM with a revised convective triggering function. *Journal of Advances in Modeling Earth Systems*, *11*, 2290–2310. https://doi.org/10.1029/2019ms001702

Xu, K. M., Arakawa, A., & Krueger, S. K. (1992). The macroscopic behavior of cumulus ensembles simulated by a cumulus ensemble model. *Journal of the Atmospheric Sciences*, *49*, 2402–2420. https://doi.org/10.1175/1520-0469(1992)049<2402:tmboce>2.0.co;2

Zhang, C., Xie, S., Tao, C., Tang, S., Emmenegger, T., Neelin, J. D., et al. (2020). The ARM data-oriented Metrics and diagnostics package for climate models: A new tool for evaluating climate models with field data. *Bulletin of the American Meteorological Society*, *101*(10), E1619–E1627. https://doi.org/10.1175/bams-d-19-0282.1

Zhang, G. J., & McFarlane, N. A. (1995). Sensitivity of climate simulations to the parameterization of cumulus convection in the Canadian climate centre general circulation model. *Atmosphere-Ocean*, *33*, 407–446. https://doi.org/10.1080/07055900.1995.9649539